

Searches for sterile component with solar neutrinos and KamLAND

P. C. de Holanda^{1,2} and A. Yu. Smirnov^{1,3}

(1) *The Abdus Salam International Centre for Theoretical Physics, I-34100 Trieste, Italy*

(2) *Instituto de Física Gleb Wataghin - UNICAMP, 13083-970 Campinas SP, Brazil*

(3) *Institute for Nuclear Research of Russian Academy of Sciences, Moscow 117312, Russia*

Abstract

Possible mixing of the active and sterile neutrinos has been considered both in the single Δm^2 approximation and in the case of more than one Δm^2 . We perform global fit of the available solar neutrino data with free boron neutrino flux in the single Δm^2 context. The best fit value corresponds to zero fraction of sterile component $\eta = 0$. We get the upper bounds: $\eta < 0.26(0.64)$ at 1σ (3σ). Due to degeneracy of parameters no one individual experiment restricts η . The bound appears as an interplay of the SNO and Gallium as well as SuperKamiokande data. Future measurements of the NC/CC ratio at SNO can strengthen the bound down to $\eta < 0.5$ (3σ). If KamLAND confirms the LMA solution with its best fit point a combined analysis of the KamLAND and solar neutrino results will lead to $\eta < 0.19(0.56)$ at 1σ (3σ). We find that existence of sterile neutrino can explain the intermediate value of suppression of the KamLAND event rate: $R_{KL} \sim 0.75 - 0.90$ in the case when more than one Δm^2 is involved.

1 Introduction

Sterile neutrino, ν_s , is a *panacea* of various problems which appear from time to time in neutrino physics. Oscillation interpretation of the LSND result [1] in the context of schemes which describe the solar and atmospheric neutrino problems [2] is the long term motivation for existence of ν_s .

There are, however, other motivations to search for the sterile component. It might happen that ν_s is the right-handed component of neutrino which turns out to be light (or massless) in the context of the see-saw mechanism, as a consequence of certain symmetry [3]. Such a symmetry ($L_e - L_\mu - L_\tau$ as in [3]) can also be responsible for large or maximal lepton mixing. Sterile neutrino can be a component of multiplet of the extended gauge group, *e.g.*, E_6 [4]. Sterile neutrino - light singlet fermion - can originate from completely different sector of theory. Many extensions of the standard model predict existence of singlet fermions: ν_s can be a mirror neutrino [5], goldstino in SUSY [6], modulino of the superstring theories [7], bulk fermions related to existence of extra dimensions [8], etc..

Neutrinos are unique particles, since only they can mix with singlets of the Standard Model. This mixing can lead to coherent effects which provide high sensitivity to existence of ν_s . The mixing terms as small as ($10^{-10} - 10^{-6}$) eV can produce the observable effects and in the case of supernova neutrinos the masses can be even smaller. In a sense, neutrino mixing is a window to physics beyond the SM.

Another motivation to search for and restrict sterile component is that interpretation of certain results can be changed strongly if one admits even very small admixture of sterile neutrinos. This concerns with the neutrinoless double beta decay, CP-violation, generation of maximal/large flavor mixing [9], etc..

So, we deal with long term program of searches for sterile neutrinos and improvements of the bounds on mixing of sterile neutrinos with all possible masses.

In this paper we will consider in details searches for sterile component in the solar neutrino flux. First detailed discussion of signatures of the sterile neutrinos have been done in [10, 11, 12] where it was marked, in particular, that studies of the spectrum distortion can reveal existence of ν_s .

There were a number of fits of the solar neutrino data in terms of pure $\nu_e \rightarrow \nu_s$ sterile conversion, but recent SNO results [13, 14] exclude pure $\nu_e \rightarrow \nu_s$ conversion at high confidence level. Still partial transformation of ν_e in ν_s is possible. The effects, and allowed fraction of sterility depend on specific scheme of mixing. Most of recent studies have been done in a single Δm^2 context: according to which the electron neutrino mixes with the state being the combination of the active (ν_μ and ν_τ) and sterile neutrino. Fraction of sterility is described by the parameter η . In [15] it was marked that η is weakly restricted provided that the original boron neutrino flux is substantially larger than the SSM flux. Global fit of the solar neutrino data [16] gives $\eta < 0.25$ (0.6) at 1σ (3σ) level. If the boron neutrino flux

is fixed according to the SSM with corresponding uncertainties the bound becomes stronger at the 3σ level: $\eta < 0.5$ [17].

In this paper we will consider effects of sterile neutrinos and bounds on sterility from the existing and future experiments. In particular, we study how combined analysis of the KamLAND and solar neutrino data can improve the bound. We generalize the analysis for the case when more than one Δm^2 is relevant. We discuss how presence of sterile component can change predictions for KamLAND rate.

The paper is organized as follows. In section 2 we consider the mixing the sterile neutrino in a single Δm^2 context. In section 3 we perform global fit of all solar neutrino data, and put bounds on the sterile fraction η . In section 3.2 we identify the data sensitive to η . In section 4 we study how future experiments can improve the bound. We consider precision NC measurements at SNO (section 4.1) and combined analysis of KamLAND and solar neutrino data (section 4.2). In section 5 we consider the ν_s mixing in the case when more than one Δm^2 is relevant. We discuss how the presence of sterile component can change predictions for the KamLAND experiment. We present our conclusions in section 6.

2 Mixing of sterile neutrinos

In what follows we will consider the case of one sterile neutrino. In general, fourth neutrino may have an arbitrary mass and sterile component can mix with all three active neutrinos. So, the scheme will have 4 new real parameters: the mass m_4 and 3 mixing angles. Situation can, however, be simplified if one takes into account existing bounds on mixing of active neutrinos. We will consider the 4-neutrino schemes which explain the solar and atmospheric neutrino data. We assume that two mass eigenstates, ν_1 and ν_2 , are split by the solar $\Delta m^2 < \text{several} \times 10^{-4} \text{ eV}^2$. We will call them the “solar pair”. Then the state ν_3 , is split from the solar pair or from ν_4 by the atmospheric mass split: $\Delta m_{atm}^2 \sim (2 - 3) \cdot 10^{-3} \text{ eV}^2$. We define the mixing matrix, $||U_{\alpha i}||$ as the unitary matrix which connects the flavor and the mass eigenstates: $\nu_\alpha = \sum_i U_{\alpha i} \nu_i$, $\alpha = e, \mu, \tau, s$, $i = 1, 2, 3, 4$.

2.1 Single Δm^2 case

As far as solar neutrinos are concerned, mixing of the electron neutrinos plays crucial role.

Let us first assume that $U_{e3} = U_{e4} = 0$, so that the electron flavor is distributed only in the “solar pair of states”: In fact, there is a strong upper bound on U_{e3} from CHOOZ experiment [19], and strong bound on U_{e4} from BUGEY experiment [20] if corresponding Δm^2 is large.

Since only U_{e1} and U_{e2} are non-zero the orthogonality conditions for ν_e and other neu-

trinos, ν_μ , ν_τ , ν_s can be written as

$$U_{e1}^\dagger U_{\alpha 1} + U_{e2}^\dagger U_{\alpha 2} = 0, \quad \alpha = s, \mu, \tau. \quad (1)$$

From these equations we get immediately:

$$\frac{U_{\mu 2}}{U_{\mu 1}} = \frac{U_{\tau 2}}{U_{\tau 1}} = \frac{U_{s 2}}{U_{s 1}} = -\frac{U_{e 2}^\dagger}{U_{e 1}^\dagger}. \quad (2)$$

That is, all non-electron flavor components enter ν_1 and ν_2 in the same combination. Indeed, let ν_x be the combination of the non-electron neutrinos which mixes with ν_e in ν_1 :

$$\nu_1 = \cos \theta_{12} \nu_e - \sin \theta_{12} \nu_x, \quad \nu_x = \frac{1}{\sqrt{1 - U_{e1}^2}} \sum_{\alpha} U_{\alpha 1} \nu_{\alpha}, \quad (3)$$

where $\sin \theta_{12} = \sqrt{1 - U_{e1}^2}$. Similarly, let ν_y be the combination of the non-electron neutrinos which mixes with ν_e in ν_2 :

$$\nu_2 = \sin \theta_{12} \nu_e + \cos \theta_{12} \nu_y, \quad \nu_y = \frac{1}{\sqrt{1 - U_{e2}^2}} \sum_{\alpha} U_{\alpha 2} \nu_{\alpha}. \quad (4)$$

Then according to (2), we have:

$$\nu_x = \nu_y. \quad (5)$$

Thus, the scheme is reduced exactly to the two two neutrino case: ν_e mixes with ν_x in the states ν_1 and ν_2 and the mixing angle equals θ_{12} .

The state ν_x can be written as

$$\nu_x = \sqrt{1 - \eta} \nu_a + \sqrt{\eta} \nu_s, \quad (6)$$

where ν_a is the combination of active (non-electron) neutrinos, ν_μ and ν_τ :

$$\nu_a = \frac{1}{\sqrt{1 - U_{s1}^2}} (U_{\mu 1} \nu_\mu + U_{\tau 1} \nu_\tau). \quad (7)$$

So, $\sqrt{\eta}$ describes admixture of sterile neutrino in the state ν_x to which ν_e can be transformed. According to (3), (4) and (6), admixtures of the sterile component in ν_1 and ν_2 equal

$$U_{s1} = \sqrt{\eta} \sin \theta_{12}, \quad U_{s2} = \sqrt{\eta} \cos \theta_{12}, \quad (8)$$

and consequently,

$$|U_{s1}|^2 + |U_{s2}|^2 = \eta. \quad (9)$$

That is, η gives total fraction of the sterile component in the solar pair.

We have proven that if the electron neutrino is distributed in two mass eigenstates only, then independently of other mixings and masses, the effect of sterile component in solar neutrinos is described by one parameter only, which is the total amount of sterile component in these two mass eigenstates.

2.2 Conversion probabilities and observable fluxes

Let us consider the oscillation effects. We introduce

$$P_{ee} = P_{ee}(\Delta m_{12}^2, \theta_{12}, V_{ex}) \quad (10)$$

- the ν_e survival probability in the system of mixed neutrinos $\nu_e - \nu_x$. Here $V_{ex} = V_e - V_\mu(1 - \eta)$ is the effective potential. According to (3) and (6) the transition probabilities of the electron neutrino to the sterile, P_{es} , and active, P_{ea} , components in terms of P_{ee} equal

$$\begin{aligned} P_{es} &= \eta(1 - P_{ee}) \\ P_{ea} &= (1 - \eta)(1 - P_{ee}). \end{aligned} \quad (11)$$

Using these probabilities we can write the fluxes of neutrinos which determine the rates of events of different types. Let us introduce f_B , the original boron neutrino flux in units of the SSM flux, :

$$f_B \equiv \frac{F_B}{F_B^{SSM}}. \quad (12)$$

Here the SSM boron neutrino flux is taken to be $F_B^{SSM} = 5.05 \cdot 10^6 \text{ cm}^{-2} \text{ s}^{-1}$. Then the elastic scattering events (ES) (detected by SuperKamiokande and SNO), the neutral current (NC) and charged current (CC) event rates at SNO are determined by the following fluxes:

$$\Phi_{CC} = f_B P_{ee}, \quad (13)$$

$$\Phi_{NC} = f_B [P_{ee} + (1 - \eta)(1 - P_{ee})], \quad (14)$$

$$\Phi_{ES} = f_B [P_{ee} + r(1 - \eta)(1 - P_{ee})], \quad (15)$$

where $r = 0.16$ is the ratio of the $\nu_{\mu,\tau} e^-$ and $\nu_e e^-$ elastic scattering cross sections. The equations (14) depend on three parameters, f_B , P_{ee} and η via two combinations

$$x \equiv f_B P_{ee}, \quad y \equiv f_B (1 - \eta)(1 - P_{ee}). \quad (16)$$

In terms of variables x and y , the fluxes can be rewritten as

$$\Phi_{ES} = x + ry, \quad \Phi_{CC} = x, \quad \Phi_{NC} = x + y. \quad (17)$$

Excluding x and y we get relation between the fluxes [15]:

$$\Phi_{ES} = \Phi_{CC} + r(\Phi_{NC} - \Phi_{CC}) = \Phi_{CC}(1 - r) + r\Phi_{NC} \quad (18)$$

which has a simple interpretation (see the first equality): the flux measured in the neutrino-electron scattering equals the flux of electron neutrinos at the detector plus the flux of non-electron active neutrinos, $\Phi_{NC} - \Phi_{CC}$, suppressed by r . The equality (18) is well satisfied in the experiment.

The equalities (17) imply the *degeneracy of parameters* [15]: different values of the original parameters f_B , η , P_{ee} lead to the same observables provided that they keep to be constant the combinations x and y . In particular, changes of η can be compensated by corresponding variations of P_{ee} and f_B , so that the combinations and therefore the observables are not changed. Clearly this is possible if P_{ee} does not depend on the energy or time. Therefore the energy and the time variations of the probability break the degeneracy. In other words, time variations and distortion of the spectrum are, in general, sensitive to the fraction of sterile neutrinos. Since no significant distortion or variations have been found experimentally, the present data have no strong sensitivity to the fraction η as we will see from exact calculations in the sect. 3.

3 Global fit and bounds on fraction of sterile component

3.1 Global analysis

We have performed a global analysis of all available solar neutrino data taking into account possible presence of the sterile component. We follow the procedure described in our previous publication [21] where details can be found, and here we summarize the main ingredients of the analysis.

We use the same data sample as in [21], which consists of

- three total rates: 1) the Ar -production rate, Q_{Ar} , from Homestake [22], 2) the Ge -production rate, Q_{Ge} from SAGE [24] and 3) the combined Ge -production rate from GALLEX and GNO [25];
- 44 data points from the zenith-spectra measured by Super-Kamiokande [26] during 1496 days of operation;
- 38 day-night spectral points from SNO [13, 14].

All solar neutrino fluxes (but the boron neutrino flux) are taken according to SSM BP2000 [28]. We use the boron neutrino flux as free parameter. For the hep -neutrino flux we take fixed value $F_{hep} = 9.3 \times 10^3 \text{ cm}^{-2} \text{ s}^{-1}$ [28, 29].

In contrast to [21], the neutrino scheme includes now mixing with sterile component which is described by the parameter η (6). So, there are three oscillation parameters: the mass squared difference, Δm^2 , and two mixings: $\tan^2 \theta$ and η . Consequently, in the free boron neutrino flux fit we have four parameters: Δm^2 , $\tan^2 \theta$, η and f_B , and therefore there are $81(\text{data points}) - 4 = 77$ d.o.f..

We perform the χ^2 test of the oscillation solution by calculating

$$\chi_{global}^2 = \chi_{rate}^2 + \chi_{SK}^2 + \chi_{SNO}^2, \quad (19)$$

η	0.0	0.2	0.4	0.6
χ^2	65.1	65.5	67.5	72.6
$\Delta m^2 (\times 10^{-5})$	6.3	5.5	4.6	4.0
$\tan^2 \theta$	0.41	0.35	0.30	0.26
f_B	1.046	1.188	1.356	1.570

Table 1: Minimum χ^2 for different values of η . Also presented are the values of parameters Δm^2 , $\tan^2 \theta$ and η that minimize χ^2 .

where χ_{rate}^2 , χ_{SK}^2 and χ_{SNO}^2 are the contributions from the total rates, the Super-Kamiokande zenith spectra and the SNO day and night spectra correspondingly. Each of the entries in (19) is the function of four parameters (Δm^2 , $\tan^2 \theta$, f_B , η), in particular,

$$\chi_{global}^2 = \chi_{global}^2(\Delta m^2, \tan^2 \theta, f_B, \eta). \quad (20)$$

We perform the global analysis for various *fixed* values of η . We first find the best fit points for a given η minimizing χ_{global}^2 with respect to Δm^2 , $\tan^2 \theta$ and f_B . This gives $\chi_{min}^2(\eta)$. The results are shown in the Table 1. The best fit corresponds to zero value of sterile fraction and $f_B = 1.05$. So, the absolute minimum is characterized by $\chi_{min}^2(0)$. According to the Table 1, χ^2 increases with η , and moreover, the increase is fast for $\eta > 0.3$. $\Delta\chi^2 = \chi_{min}^2(0.4) - \chi_{min}^2(0) = 2.4$; for $\eta = 0.6$ this difference is $\Delta\chi^2 = 7.5$.

Then we construct the 3σ regions in the $\Delta m^2 - \tan^2 \theta$ plane (Fig. 1) minimizing $\chi^2(\Delta m^2, \tan^2 \theta, f_B)$ with respect to f_B : we denote the corresponding minimal value of χ^2 by $\chi_f^2(\Delta m^2, \tan^2 \theta)$. Then 3σ contours are determined by $\chi_f^2(\Delta m^2, \tan^2 \theta) - \chi_{min}^2(\eta) = 11.73$, where $\chi_{min}^2(\eta)$ is the minimum χ^2 for a given value of η . We have found also lines of constant values of f_B which minimize χ^2 for a given η .

According to Fig. 1 and the Table 1, with increase of η the allowed region shifts to smaller values of $\tan^2 \theta$ and Δm^2 . At the same time f_B and χ_{min}^2 increase.

These features can be well understood using Eqs. (15 - 16). Increase of η [decrease of $(1 - \eta)$] can be compensated by increase of f_B and decrease of P_{ee} . Since $P_{ee} \sim \sin^2 \theta$, the decrease of P_{ee} implies decrease of mixing angle. With decrease of mixing the distortion of the spectrum (mainly the turn up of the probability at low energies) becomes stronger. This leads to shift of the allowed region to smaller values of Δm^2 (shift of the spectrum from the adiabatic edge).

Let us consider breaking of parameter degeneracy. Taking $P_{ee} \approx \sin^2 \theta$ in expressions (16) and using results of the Table 1 we find values of parameters $x(\eta)$ and $y(\eta)$ for different η in the best fit points (see Table 3.1). As follows from the Table 3.1 in the best fit points the parameters $x(\eta)$ and $y(\eta)$ are not invariant under changes of η : x slightly increases (by 5%) whereas y decreases significantly: almost by 50%. Another way to see these variations

η	0.0	0.2	0.4	0.6
x	0.304	0.308	0.313	0.320
y	0.742	0.703	0.623	0.492
$y(x = \text{const})$	0.726	0.694	0.622	0.500

Table 2: Values of parameters x and y in the best fit points of global analysis for different values of η .

is to keep $x = \Phi_{CC} = \text{constant}$ and to exclude P_{ee} from the combination y :

$$y = (1 - \eta)(f_B - \Phi_{CC}). \quad (21)$$

Using $\Phi_{CC} = 0.32$ we find $y(\eta)$ shown in the third line of the Table 3.1. Thus, the invariance of x and y (and therefore a degeneracy) is broken which leads the dependence of χ^2_{\min} on η and therefore to sensitivity of the analysis to the presence of sterile neutrinos.

For fixed values of η and f_B we minimize χ^2 with respect to $\Delta m^2, \tan^2 \theta$ which gives $\chi^2_{\Delta, \theta} = \chi^2_{\Delta, \theta}(\eta, f_B)$. Using this function we construct contours of constant confidence level in η, f_B plane (fig. 2). From this figure we get an upper limit for the sterile fraction

$$\eta < 0.38 (0.70), \quad 1\sigma (3\sigma) \quad (22)$$

The boron neutrino flux which correspond to maximal allowed value of η equals $f_B = 1.25$ (1σ) and $f_B = 1.68$ (3σ).

We have performed minimization of χ^2 with respect to $\Delta m^2, \tan^2 \theta$ and f_B , thus finding $\chi^2_{\Delta, \theta, f_B} = \chi^2(\eta)$. Then the function $\chi^2(\eta)$ allows to put the bounds for 1 d.o.f.:

$$\eta < 0.26 (0.64), \quad 1\sigma (3\sigma) \quad (23)$$

These results are very similar to results obtained in [16, 17]. In particular, it was found [16] that at 1σ : $\eta_{\max} = 0.25$ for $f_B \sim 1.25$, and at 3σ : $\eta_{\max} = 0.6$ for $f_B \sim 1.75$.

Imposing the SSM bound on the neutrino flux further strengthen the bound on “sterility”. It was found in [17]: $\eta < 0.25$ at the 1σ and $\eta < 0.5$ at the 3σ level. Notice that in fact 1σ bound is unchanged since at this level the required boron neutrino flux is within 1σ SSM prediction. In contrast, the limit becomes stronger at the 3σ level, where substantially larger than in SSM flux is needed.

For the SSM value of the boron neutrino flux, $f_B = 1$, we get from the fig. 2 the following bounds on the sterile fraction: $\eta < 0.14$ (1σ), $\eta < 0.30$ (2σ), $\eta < 0.47$ (3σ).

3.2 Who does not like sterile neutrino?

Let us identify observables which are sensitive to η . As we have discussed in sect. 2.1 these observables should contain information about the time variations or/and the energy

dependence of the conversion effect. These dependences remove the degeneracy and therefore restrict η .

No statistically significant time variations have been found although some indications of the Day- Night asymmetry, A_{ND} , exist [26, 14]. Let us consider if A_{ND} can restrict the admixture of sterile neutrino. The high energy neutrino data can be described by the ν_e -survival probability during the day and during the night: P_{ee}^D, P_{ee}^N , or equivalently, by $\Delta P_{ee} \equiv P_{ee}^N - P_{ee}^D$ and $\bar{P}_{ee} \equiv (P_{ee}^N + P_{ee}^D)/2$. Consequently, in Eq. (13 - 15) we should substitute $P_{ee} \rightarrow \bar{P}_{ee}$ and add to analysis an additional observable:

$$A_{ND} = \frac{\Delta P_{ee}}{\bar{P}_{ee}}. \quad (24)$$

In the LMA region the average suppression is determined basically by mixing angle: $\bar{P}_{ee} \sim \sin^2 \theta$, whereas the DN asymmetry depends mainly on Δm^2 . This can be seen from lines of constant ratio $CC/NC \sim P_{ee}$ and lines of constant A_{ND} which are nearly orthogonal each other (see figs. 5 and 6 from [21]). Therefore ΔP_{ee} and \bar{P}_{ee} do not correlate and can be considered as independent fit parameters. For a given \bar{P}_{ee} , the difference ΔP_{ee} can change in the wide range, and the data on the asymmetry can be easily fitted. So, adding experimental information about the Day and Night asymmetry does not help to resolve degeneracy and therefore to improve the bound on η . Precise measurements of the zenith angle dependence of signal will change this conclusion.

No statistically significant distortion of the energy spectrum is found for $E > 5$ MeV, which supports the degeneracy problem. The distortion (in experiments sensitive to $E > 5$ MeV) is expected for higher values of Δm^2 and small mixing. However, substantial distortion is expected over wider detectable energy range which includes also the pp - neutrinos. Therefore, the interplay of the high energy data and results from the low energy experiments should break the degeneracy.

To illustrate this effect, let us describe the distortion by two (for simplicity) different values of probabilities: at high energies, P_{ee}^H , and at low energies, P_{ee}^L ($E < 0.5$ MeV). The signal in the Gallium experiment is determined essentially by P_{ee}^L : so that the Ge -production rate equals $Q_{Ge} \propto P_{ee}^L$, and obviously, no substantial dependence on f_B appears. In contrast to the Day-Night asymmetry case, the probabilities P_{ee}^L and P_{ee}^H are strongly (anti) correlated. Indeed, in the range of pp -neutrinos:

$$P_{ee}^L \sim 1 - 0.5 \sin^2 2\theta, \quad (25)$$

and since $P_{ee}^H \approx \sin^2 \theta$ we get

$$P_{ee}^L \sim 1 - 2P_{ee}^H(1 - P_{ee}^H). \quad (26)$$

With decrease of P_{ee}^H the low energy probability P_{ee}^L increases. Consequently, the predicted value of the Ge -production rate increases. Thus, combination of the Gallium and SNO data should break the degeneracy of parameters.

η	0.0	0.2	0.4	0.6
χ^2	25.6	25.4	25.3	25.1
$\Delta m^2 (\times 10^{-5})$	4.5	4.5	4.0	3.6
$\tan^2 \theta$	0.45	0.35	0.28	0.18
f_B	1.039	1.201	1.432	2.013

Table 3: Minimum χ_{SNO}^2 for different values of η . Also presented are values of parameters Δm^2 , $\tan^2 \theta$ and η that minimize the χ_{SNO}^2 .

Now let us describe results of exact numerical calculations.

1). We have performed the χ^2 analysis of the SNO data only. The best fit points in the oscillation plane as well as f_B which minimize $\chi_{SNO}^2(\eta)$ are given for different values of η in the Table 3.2. Notice that with increase of η the quality of the fit does not change: χ^2 even slightly decreases. So, as far as SNO data alone are concerned, no bound on η appears. Variations of η can be completely compensated by changes of P_{ee} and f_B . The day-night asymmetry has low statistical significance.

The SNO experiment has higher sensitivity to the NC - events. For this reason the allowed region provided by SNO is restricted in $\tan^2 \theta$ from both sides. Increase of η has the effect of moving the allowed region to smaller values of $\tan^2 \theta$, as can be seen in fig. 3.

Indeed, to keep the combinations (16) unchanged with increases of η one needs (i) to diminish P_{ee} , which implies decrease of θ since in the LMA region $P_{ee} \sim \sin^2 \theta$, (ii) to decrease Δm^2 to avoid distortion (turn up) of the spectrum at small energies and (iii) to increase f_B to compensate decrease of P_{ee} .

2). In fig. 3 we show also lines of constant Ge -production rate. The rate increases with decrease of mixing. According to the figure, in the SNO allowed region for $\eta = 0.6$ the rate $Q_{Ge} > 75$ SNU and in the best fit point $Q_{Ge} = 83$ SNU. For $\eta = 0.4$ we get $Q_{Ge} = 75$ SNU in the best fit point. The combined results from SAGE, Gallex and GNO experiments is $Q_{Ge} = (70 \pm 4)$ SNU. So, the Gallium results prevent from further shift of the allowed region to smaller θ_{12} and therefore forbid larger η . To illustrate the role of Gallium experiments, we find the bounds on η that can be derived by taking only SNO and Gallium data:

$$\eta < 0.43 (0.78), \quad 1\sigma (3\sigma), \quad (27)$$

which are weaker than those obtained by taking all the data (23).

In principle, further more precise measurements of the Ge -production rate could improve the bound on the sterile component.

3). Let us comment on the impact of SuperKamiokande. In fig. 4 we show result of analysis of the SuperKamiokande data only for different values of η . The excluded (at

1σ) regions in the oscillation parameter space are due to the effects of spectrum distortion and the Earth ν_e regeneration. They are only slightly modified by the presence of sterile component. With increase of η the excluded region shifts to larger mixing angles. This is related to the fact that with increase of sterile fraction the distortion of the spectrum increases due to decrease of the damping effect related to active neutrinos. The exclusion due to earth regeneration becomes weaker. Since for active-sterile system the effective matter potential is smaller the regeneration region shifts to smaller Δm^2 . Correspondingly, lower bound of the allowed region shifts to smaller Δm^2 .

In the allowed region, where distortion and time variations are small the data can be reproduced for different values of η by adjusting f_B and P_{ee} (see (15)).

In fig. 4 we show also f_B that gives the best fit to the Super-Kamiokande data. With increase of η the lines $f_B = const$ shift to larger $\tan^2\theta$ and Δm^2 (where the survival probability is larger) to compensate decrease of muon and tau neutrino contribution. Large values of η are allowed, when the boron neutrino flux is much larger than the SSM flux.

Similarly to the Gallium experiments, SuperKamiokande prevents from the shift of the allowed region to smaller mixings. Consequently, the combined fit of the SNO and SK will also give the bound on the sterile fraction. Comparison of the bounds (23) with and (27) without the SK result allows to evaluate the role of SuperKamiokande.

4). The Homestake experiment alone is not sensitive to η . However, it has some impact since its result restrict the oscillation parameters. The Ar -production rate decreases with mixing angle and the agreement with the Homestake result becomes even better with increase of η . Comparing the SNO and Homestake results we find that in the best fit SNO point for $\eta = 0.6$ the rate equals $Q_{Ar} = 2.75$ SNU which is within 1σ of the Homestake result. So, the SNO and Homestake data favor presence of sterile component.

Summarizing, the bound on sterility appears as combined effect of several experiments. In the global analysis the constrain on η comes from the SNO measurements of the spectrum which contains information about the NC and CC event rate from the one hand side and Gallium as well as the SK experiment from the other side. With increase of η , SNO pushes the allowed region to smaller $\tan^2\theta$, whereas Gallium and SK experiments put lower bound on $\tan^2\theta$. For instance, the best SNO fit point for $\eta = 0.6$ lies in the excluded Gallium region and at the border of the SK excluded region.

4 Future experiments and bounds on η

4.1 NC measurements at SNO

SNO is taking data with much higher sensitivity to the NC current events, and therefore precision of measurements of Φ_{NC} will be significantly improved. Clearly, distortion of the spectrum of the NC events will be signature of the sterile neutrino conversion. Although if LMA is the dominant solution, one does not expect observable effect. As far as total rate is concerned, the parameters can be adjusted in such a way that even more precise data can be reproduced for large η . Basically we will get the same shift of the allowed region as in fig. 1 but the size of the region around the the best fit point will be smaller. For this reason no drastic improvements of the bound on sterility is expected.

To evaluate the impact of future NC -measurements at SNO we show in fig. 5 the 1σ region of predictions of Φ_{NC} as a function of η from the global fit. The results have been obtained in the following way. We use the global analysis of the solar neutrino data for different values of η , as is shown in fig. 1. Then we calculate Φ_{NC} in the best fit points (solid line) as well as the spread of predictions for Φ_{NC} within 1σ allowed region. Using the fig. 5, we find that the present 1σ experimental result on Φ_{NC} , gives the upper bound $\eta < 0.7$ which agrees with the 3σ bound from the global analysis. Assuming three times smaller error bars for the NC measurements, $\Phi_{NC} = 1 \pm 0.03$, we get the bound $\eta < 0.5$ which should be compared with present bound $\eta < 0.64$.

4.2 KamLAND and sterile fraction

The signal at KamLAND is determined by the vacuum oscillation survival probability, so that the rate of events is

$$N = \sum_i \int dE \left(1 - \sin^2 2\theta_{12} \sin^2 \frac{\Delta m_{12}^2 L_i}{2E} \right) F_i \sigma A, \quad (28)$$

where F_i is the flux from i reactor, σ is the cross-section of $\bar{\nu}p \rightarrow e^+n$ reaction, A is the energy resolution function. The sum is taken over all reactors contributing to the flux at Kamioka and the integral denotes schematically the integrations over the neutrino energy, and the true energy of produced positron. This rate does not depend on η or f_B . Being combined with the solar neutrino results it breaks degeneracy. KamLAND will fix the oscillation parameters Δm_{12}^2 , $\tan^2 \theta_{12}$, and consequently, will allow to predict P_{ee} which describes the solar neutrino conversion.

Let us evaluate how combined analysis of the solar data and KamLAND can improve the bound on sterile component.

Let us introduce the suppression factor of total event rate above certain threshold:

$$R_{KL}(\Delta m^2, \tan^2 \theta) \equiv \frac{N(\Delta m^2, \tan^2 \theta)}{N_0}, \quad (29)$$

where N is given in (28) and N_0 is the event rate in absence of oscillations.

Since predictions for KamLAND do not depend on the state to which the electron neutrino converts, we can use results of calculations of R_{KL} for the pure active case [21]. In fig. 8 of paper [21] we have presented lines of constant R_{KL} in $(\Delta m^2, \tan^2 \theta)$ plane. In the best fit points we find $R_{KL}(0) = 0.66$, $R_{KL}(0.2) = 0.63$, $R_{KL}(0.4) = 0.55$, $R_{KL}(0.6) = 0.52$. Due to decrease of Δm^2 in the best fit points, the expected value of the suppression in the KamLAND experiment becomes stronger.

To quantify impact of the event rate measurements at KamLAND we have constructed the $\chi^2(\Delta m^2, \tan^2 \theta, f_B, \eta)$ as the function R_{KL} . Practically we impose the following condition $R_{KL}(\Delta m^2, \tan^2 \theta) = const$ which implies relation between Δm^2 and $\tan^2 \theta$. So, for a given value R_{KL} the χ^2 is the function of Δm^2 or $\tan^2 \theta$ only:

$$\chi^2 = \chi^2(\tan^2 \theta, R_{KL}, f_B, \eta). \quad (30)$$

For each value of R_{KL} we minimize χ^2 with respects to $\tan^2 \theta, f_B, \eta$ thus finding $\chi_{\theta, f_B, \eta}^2(R_{KL})$. This function is shown in the upper panel of fig. 6. In the bottom panel the corresponding values of f_B and η , which minimize χ^2 , are presented. For comparison in the upper panel we show also the function $\chi_{\theta, f_B}^2(R_{KL})$ for $\eta = 0$.

The following remarks are in order.

For $R_{KL} < 0.67$ the quality of the fit does not depend on R_{KL} . It corresponds to $\eta = 0$ and $f_B \approx 1.05$. For $R_{KL} > 0.67$, χ^2 increases with R_{KL} . Simultaneously the best fit values of η and f_B increase. At 3σ level ($\chi^2 = 74$) we find maximal value of R_{KL} and corresponding values of η and f_B

$$R_{KL} \sim 0.75, \quad \eta = 0.35, \quad f_B = 1.4. \quad (31)$$

For $\eta = 0$ the value $R_{KL} \sim 0.725$ is allowed. So, the introduction of sterile neutrino in the single Δm^2 approach does not lead to significant increase of maximal allowed value of R_{KL} . The goodness of the fit decreases sharply: *e.g.* for $R_{KL} = 0.8$ we get $\Delta\chi^2 = 25$ even in presence of sterile component.

Let us analyze how the KamLAND spectral measurements can help in constraining η . We have simulated the KamLAND spectral data for 4 different points a), b), c), d) in the $\Delta m^2 - \tan^2 \theta$ plane (marked by stars in fig. 7a)). In simulations we use statistics which can be collected during 3 years in 600 tons above the energy threshold for visible energy $E_{vis} = 2.6$ MeV. In absence of oscillations this would correspond to 1170 events. We assumed a 4% uncertainty in the overall normalization and a 2% uncertainty in the energy scale. We have simulated the energy spectrum (for each point) using 12 bins of 0.5 MeV size in the visible energy.

We perform χ^2 analysis of simulated spectra assuming a full correlation of systematics uncertainties. We minimize

$$\chi_{KL}^2 = \sum_{i=1,12} \sum_{j=1,12} R_i \sigma_{i,j}^{-2} R_j \quad (32)$$

and construct contours of constant 1σ , 2σ , 3σ confidence level around selected points in the $\Delta m^2, \tan^2 \theta$ plane (see fig. 7a). Notice that our allowed regions are somehow larger than those obtained in [31, 32, 35], since we include systematic errors and also use higher threshold (smaller number of events). In agreement with results of calculations of other groups [31, 32, 35] we find that KamLAND will be able to measure Δm^2 rather precisely (if $\Delta m^2 < 2 \cdot 10^{-4} \text{ eV}^2$). At the same time determination of the mixing angle will not be very accurate. For the present best fit point (b) we get from the figure $\tan^2 \theta = 0.28 - 0.60$ at the 1σ level, and $\tan^2 \theta = 0.25 - 0.85$ at the 3σ level.

Then we have performed combined analysis of the existing solar and simulated KamLAND data (notice that by the time KamLAND will have 3 years statistics new solar neutrino data will appear). For each selected point of the oscillation parameters in fig. 7a we calculate a global χ_{tot}^2 , which includes contributions from the solar neutrino analysis, χ_{Sun}^2 , and the KamLAND, χ_{KL}^2 :

$$\chi_{tot}^2 = \chi_{KL}^2(\tan^2 \theta, \Delta m^2) + \chi_{Sun}^2(\tan^2 \theta, \Delta m^2, \eta, f_B) . \quad (33)$$

For each value of η we minimize χ_{tot}^2 with respect to Δm^2 , $\tan^2 \theta$ and f_B . Results of this minimization as a function of η are presented in fig. 7b. Let us comment on results for four selected points.

The point b) is the best fit point of the global fit which corresponds to $\eta = 0$. As follows from the figure,

$$\eta < 0.19 \text{ (0.56)} \quad 1\sigma \text{ (3}\sigma\text{)}, \quad (34)$$

thus improving the bound (23) from the solar data analysis only.

The points c) and d) are at larger Δm^2 and $\tan^2 \theta_{12}$ as compared with b) thus further removed from the region preferred in the case of non-zero sterile component (small Δm^2 and $\tan^2 \theta_{12}$). If KamLAND selects these points the bound on sterile component will be stronger than in a): $\eta < 0.09$ (0.45) at 1σ (3σ).

The point a) is in the region preferable by sterile component. Selecting this point KamLAND will favor non-zero η . From the lower panel we get: $\eta = 0.36_{-0.12}^{+0.16}$ at 1σ and $\eta > 0$ at 2σ level. The 1σ lower bound is $\eta > 0.24$.

For the points a) - d) we get the upper bounds on η : $\eta < 0.08$ (c and d), 0.19 (b) and 0.52 (a). We have performed similar analysis for all the points of the oscillation parameter space. We show in fig. 8 the results as lines of constant upper bounds in the oscillation parameter plane. As a tendency, the bound becomes weaker with decrease of mixing and Δm^2 . For sufficiently small $\tan^2 \theta$ the best fit corresponds to a non-zero value of η and the lower bound on η appears. In the lower panel of fig. 8 we show such a lower limit for all

points in $(\Delta m^2, \tan^2 \theta)$ plane.

5 Beyond single Δm^2 context

The results described in the previous sections can change if the electron neutrino mixes in the other mass eigenstates beyond the solar pair. Now more than one Δm^2 is involved, and effect depends on specific values of additional Δm^2 .

In what follows we will assume that mixing of ν_e in the states ν_3 and ν_4 is small. Then if additional Δm^2 are outside the range of the MSW enhancement (*e.g.* Δm_{14}^2 is large) the effect of new ν_e mixing is small being suppressed by the mixing itself. If, however, Δm_{14}^2 is in the range of the MSW enhancement, the effect of additional mixing can be large. We will consider both possibilities.

5.1 Large additional Δm^2

Suppose ν_e has non-zero admixture in ν_3 characterized by $U_{e3} = s_{13}$. (Recall that ν_3 is separated from the solar neutrino pair by the mass gap which corresponds to the atmospheric neutrino split.) We assume that ν_e -admixture in ν_4 is negligible so that the mass of ν_4 can be arbitrary within the allowed range by non-solar neutrino experiment. We assume also that in the limit $s_{13} \rightarrow 0$, the state ν_3 coincides with ν'_a - the combination of ν_μ and ν_τ , which is orthogonal to ν_a (7). In turn, ν_4 is the combination of ν_s and ν_a . As a result, we get the following mixing pattern:

$$\begin{aligned}
 \nu_1 &= \cos \theta_{12}(c_{13}\nu_e - s_{13}\nu'_a) - \sin \theta_{12}\nu_x, \\
 \nu_2 &= \sin \theta_{12}(c_{13}\nu_e - s_{13}\nu'_a) + \cos \theta_{12}\nu_x, \\
 \nu_3 &= c_{13}\nu'_a + s_{13}\nu_e, \\
 \nu_4 &= \nu'_x,
 \end{aligned} \tag{35}$$

where ν_x is defined in (6) and ν'_x is the orthogonal to ν_x combination of ν_s and ν_a . The mixing (35) differs from the generic case since ν_e and ν'_a do not mix in ν_4 , and ν_a and ν_s do not mix in ν_3 .

The dynamics of propagation is similar to that of the case of three neutrinos. Indeed, let us represent ν_e in the following form:

$$\nu_e = c_{13}\nu'_e + s_{13}\nu_3, \tag{36}$$

where $\nu'_e = \cos \theta_{12}\nu_1 + \sin \theta_{12}\nu_2$ coincides with ν_x , as can be easily checked. For the energies of solar neutrinos the matter effect on s_{13} is negligible. Furthermore, the oscillations of solar

neutrinos related to ν_3 are averaged out. At the same time, ν'_e and ν_x form standard two neutrino system with vacuum mixing and mater effects.

Using these features of dynamics, as well as projection of original flavor states onto ν'_e, ν_x, ν_3 one gets immediately the conversion probabilities:

$$\begin{aligned} P_{ee} &= c_{13}^4 \tilde{P}_{ee} + s_{13}^4 \\ P_{es} &= c_{13}^2 \eta (1 - \tilde{P}_{ee}) \\ P_{ea} &= c_{13}^2 (1 - \eta) (1 - \tilde{P}_{ee}) + s_{13}^2 c_{13}^2 (1 + \tilde{P}_{ee}), \end{aligned} \quad (37)$$

where \tilde{P}_{ee} is the ν'_e -survival probability in the $\nu'_e - \nu_x$ system: $\tilde{P}_{ee} = \tilde{P}_{ee}(\theta_{12}, \Delta m_{12}^2, \tilde{V})$ and $\tilde{V} = c_{13}^2 V_e - V_\mu (1 - \eta)$. As in the previous case, the parameter η determines fraction of ν_s in the state ν_x to which ν'_e converts, and also it gives total fraction of the ν_s in the solar pair (9).

Using (37), we get fluxes (in the units of the SSM flux) measurable by different reactions:

$$\Phi_{CC} = f_B [c_{13}^4 \tilde{P}_{ee} + s_{13}^4], \quad (38)$$

$$\Phi_{NC} = f_B [1 - (1 - \tilde{P}_{ee}) \eta c_{13}^2], \quad (39)$$

$$\Phi_{ES} = f_B [c_{13}^4 \tilde{P}_{ee} + s_{13}^4 + r c_{13}^2 (1 - \tilde{P}_{ee}) (1 - \eta) + r s_{13}^2 (1 + \tilde{P}_{ee})]. \quad (40)$$

Comparing with Eq. (13,14, 15) we find that corrections are indeed of the order s_{13}^2 . For the allowed values of s_{13}^2 these corrections have small impact on the data fit, as one can see from our analysis in [21].

The fluxes Φ_{CC} , Φ_{NC} , Φ_{ES} depend on two combinations of parameters, as in Eq. (17), with substitution $x \rightarrow x'$, $y \rightarrow y'$, where

$$x' = c_{13}^4 x, \quad y' = c_{13}^2 + s_{13}^2 (x + f_B), \quad (41)$$

and x and y are defined in (16). So, the problem of degeneracy is not resolved with s_{13} corrections. Notice also that the fluxes in (38 - 40) satisfy the relation (18).

The KamLAND signal is determined by the survival probability

$$P_{ee} = c_{13}^4 P_2 + s_{13}^4, \quad (42)$$

where P_2 is the two neutrino vacuum oscillation probability determined by Δm_{12}^2 and θ_{12} . The factor c_{13}^4 leads to additional suppression of the KamLAND signal and shift of the allowed regions to smaller θ_{12} (see detailed analysis in the 3ν context in [34]).

5.2 Small additional Δm^2

Let us consider the case when even small ν_e mixing beyond the solar pair can produce a strong effect. Suppose that,

(i) ν_e mixes with ν_x in the solar pair, ν_1 and ν_2 , which has Δm_{12}^2 and $\tan^2 \theta_{12}$ in the LMA region, as in (35);

(ii) the state $\nu_4 \approx \nu'_x$ (see (35)) is heavier than ν_1 and the mass splitting is $\Delta m_{41}^2 \sim 10^{-6}$ eV². (The mass m_1 can be very small or even zero). Furthermore, ν_e has small admixture in ν_4 : $\tan^2 \theta_{14} \sim 10^{-3}$, so that $\nu_e - \nu'_x$ oscillation parameters are in the SMA region.

(iii) the admixture of ν_e in the ν_3 is zero (for simplicity).

Then, similarly to (35) we can write the mixing as

$$\begin{aligned}
\nu_1 &= \cos \theta_{12}(c_{14}\nu_e - s_{14}\nu'_x) - \sin \theta_{12}\nu_x, \\
\nu_2 &= \sin \theta_{12}(c_{14}\nu_e - s_{14}\nu'_x) + \cos \theta_{12}\nu_x, \\
\nu_3 &= c_{13}\nu'_a, \\
\nu_4 &= c_{14}\nu'_x + s_{14}\nu_e.
\end{aligned} \tag{43}$$

Here ν'_x is the combination of ν_a and ν_s orthogonal to ν_x (6), and ν'_a is the combination of ν_μ and ν_τ orthogonal to ν_a (7).

The system has two resonances associated with Δm_{12}^2 and Δm_{41}^2 . Let us estimate qualitatively the conversion effect in different energy ranges.

In the first resonance related to Δm_{12}^2 the conversion is completely adiabatic. So, at the high energies, $E > 7 - 8$ MeV, where crossing of the resonance occurs the survival probability equals $P_{ee}^H \approx \sin^2 \theta_{12}$. At low energies, $E < 0.5$ MeV, (no 12-resonance crossing) effect driven by Δm_{12}^2 is reduced to averaged vacuum oscillations. The result of conversion is similar to the one in usual three neutrino system:

$$P_{ee}^L = c_{12}^4 P'_2 + s_{12}^4, \tag{44}$$

where P'_2 is the survival probability in the resonance related to Δm_{14}^2 . It has a typical form of the survival probability of the SMA solution and characterized by Δm_{14}^2 and mixing parameter $\tan^2 \theta = \tan^2 \theta_{14} / \cos^2 \theta_{12}$. Appearance of P'_2 in this expression leads to an additional suppression of the pp -neutrino flux.

In the intermediate energy range, $E = (0.5 - 7)$ MeV, the conversion driven by Δm_{14}^2 will lead to flattening of the adiabatic edge of the suppression pit due to Δm_{12}^2 .

5.3 KamLAND result and LMA

In the best fit point of the LMA region we predict $R_{KL} = 0.66$ for zero η [21]. At 3 σ level $R_{KL} < 0.73$. In presence of the sterile component this bound can be slightly relaxed: $R_{KL} < 0.76$. For other solutions of the solar neutrino problem we predict $R_{KL} \approx 1.0$ if $s_{13} = 0$. For non-zero s_{13} the oscillations driven by Δm_{atm}^2 will lead the averaged oscillation result at KamLAND: $R_{KL} = 1 - 0.5 \sin^2 2\theta_{13}$. For maximal allowed values of s_{13} we get $R_{KL} = 0.90 - 0.95$ depending on Δm_{atm}^2 . What if $R_{KL} = 0.76 - 0.90$ will be found?

The following comments are in order:

If solution of the solar neutrino problem is in the LMA region, a strong suppression is expected in KamLAND. In this case, introduction of additional sterile states will not help in the single Δm^2 context, as we have found in the Sect. 3.

Let us discuss what happens if two or more Δm^2 contributes.

Oscillation parameters can be taken beyond the LMA region in such a way that suppression in the KamLAND experiment is weaker. In this case, however, the conversion of solar neutrinos will not describe data in the two neutrino context. Then the parameters (mass, flavor mixing) of the ν_4 can be selected in such a way that conversion driven by ν_4 will not change KamLAND result but correct description of the solar data.

Such a possibility can be realized in the scheme described in the previous section 5.2 with $\Delta m_{12}^2 \sim 6 \cdot 10^{-5} \text{ eV}^2$. Indeed the KamLAND result is determined by the oscillations driven by Δm_{12}^2 and θ_{12} . For $\tan^2 \theta_{12} \sim 0.10 - 0.15$ we get $R_{KL} = 0.80 - 0.85$.

As far as the solar neutrino signal is concerned, the high energy signal will be suppressed by $\sin^2 \theta$, so that large boron neutrino flux: $f_B \sim 1.6$ is required to explain the SNO and SK results. According to our previous consideration, in the single Δm^2 context this point would be excluded by the Gallium experiment (large Q_{Ge}) and by SK (distortion of spectrum). The effect of Δm_{14}^2 changes a situation: appearance of P_2' in expression for probability at low energies (44) leads to an additional suppression of the pp -neutrino flux, and consequently, Q_{Ge} rate. In the intermediate energy range, $E = (0.5 - 7) \text{ MeV}$, the conversion driven by Δm_{14}^2 will relax the SuperKamiokande lower bound on mixing which follows from absence of spectrum distortion. The detailed analysis of this possibility will be given elsewhere [36].

Another possibility to reconcile an intermediate suppression of signal in KamLAND and explanation of the solar neutrino data is to split two problems. Suppose the solar pair has Δm_{12}^2 in the LOW or VO regions, so that it does not produce any effect in KamLAND. The state ν_4 which consists predominantly of the sterile component has the mass split: $\Delta m_{14}^2 > 10^{-4} \text{ eV}^2$. Then the suppression of the KamLAND signal is determined by admixture of ν_e in ν_4 : $R_{KL} = 0.5 \sin^2 2\theta_{14}$. For instance, $R_{KL} = 0.85$ can be achieved at $\sin^2 \theta_{14} = 0.09$. Effect in solar neutrinos will be determined by $P_{ee}^{sun} = c_{14}^4 P_{ee} + s_{14}^4$, where P_{ee} is the survival probability for the conversion driven by Δm_{12}^2 . Additional factor $c_{14}^4 \sim 0.8$ can even improve the fit of the data for LOW and SMA [21].

6 Conclusions

1. We have studied properties of mixing of the sterile and active neutrinos. In the single Δm^2 context (when electron neutrino is present in two mass eigenstates only) the problem is reduced precisely to two neutrino problem with mixing of ν_e with ν_x in the solar pair (ν_x

is the combination of the active and sterile neutrinos).

2. We have performed the global fit of the solar neutrino data in the single Δm^2 context, treating the boron neutrino flux as a free parameter. The best fit corresponds to zero admixture of sterile component, $\eta = 0$. We get the upper bound $\eta < 0.26$ (0.64) at 1σ (3σ). With increase of η the best fit point shifts to smaller Δm^2 and $\tan^2 \theta_{12}$.
3. Due to degeneracy of parameters, no one single observable gives the bound on η . The bound on sterility appears as an interplay of the SNO results whose allowed region of the oscillation parameters shifts to smaller mixings and Δm^2 with increase of η and Gallium as well as SK results which restrict the mixing and Δm^2 from below.
4. Further more precise measurements of the NC event rate at SNO will strengthen the bound: $\eta < 0.5$ (3σ).
5. Implications of KamLAND depend on specific results of KamLAND measurements. If KamLAND result (rate, spectrum) corresponds to the best fit point of the solar neutrino analysis, then after 3 years of the KamLAND operation the limit will be strengthened down to $\eta < 0.19$ (0.55) at 1σ (3σ). The limit will be stronger if the KamLAND best fit point will be at larger $\tan^2 \theta_{12}$ and Δm^2 than the solar neutrino data give at present. In contrast, if KamLAND selects smaller $\tan^2 \theta_{12}$ and Δm^2 , the limit will be weaker, and moreover, the data may prefer non-zero sterile admixture.
6. The presence of sterile neutrinos (in the single Δm^2 context) relaxes the upper bound on the predicted rate R_{KL} only weakly from 0.73 to 0.76 (3σ). Larger values of R_{KL} can be reached in the two Δm^2 context.
7. If electron neutrino mixes also in other mass eigenstates, the effects depend substantially on values of other Δm^2 .

If additional $\Delta m_{14}^2 \gg \Delta m_{12}^2$ the small corrections appear to formulas with a single Δm^2 which are proportional to the mixing of ν_e in additional mass eigenstates, *e.g.*, s_{13}^2 . If Δm^2 , is in the MSW range an additional mixing can be resonantly enhanced in matter producing much larger effect. In this case intermediate values of R_{KL} can be obtained.

References

- [1] LSND Collaboration, Phys.Rev. D64 (2001) 112007.
- [2] For recent discussion see M. Maltoni, T. Schwetz, M. A. Tortola, J. W. F. Valle, Nucl. Phys. B 643, 321-338; M. C. Gonzalez-Garcia, M. Maltoni, C. Peña-Garay, Phys. Rev.D64, 093001 (2001), hep-ph/0105269.
- [3] W. Grimus and L. Lavoura, Phys. Rev D. 62 (2000) 093012; J. High Energy Phys. 09 (2000) 007, J. High Energy Phys. 07 (2001) 045; S. F. King, Nucl. Phys. B 576 (2000) 85; S. F. King and N. Singh, Nucl.Phys. B591 (2000) 3; H. S. Goh, R. N. Mohapatra, S.-P. Ng, Phys. Lett. B542 (2002) 116.
- [4] E. Ma, Phys. Lett. B 380 (1996) 286; Z. Chacko and R. Mohapatra, Phys. Rev. D 61 (2000) 053002.
- [5] R. Foot and R.R. Volkas, Phys. Rev. **D52**, 6595 (1995); Z.G. Berezhiani and R.N. Mohapatra, Phys. Rev. **D52**, 6607 (1995); V. Berezinsky and A. Vilenkin, Phys. Rev. **D62**, 083512 (2000); V. Berezinsky, M. Narayan and F. Vissani, hep-ph/0210204.
- [6] E. J. Chun, A. S. Joshipura, A. Yu. Smirnov, Phys. Rev. D54:4654 (1996).
- [7] K. Benakli, A. Yu. Smirnov, Phys. Rev. Lett. 79:4314 (1997), A. Lukas, P. Ramond, A. Romanino, G. G. Ross, Phys.Lett. B495 (2000) 136.
- [8] K. R. Dienes, E. Dudas and T. Gherghetta, Nucl. Phys. B557, 25 (1999); N. Arkani-Hamed, S. Dimopoulos, G. Dvali and J. March-Russel, Phys. Rev D 65 (2002) 024032, G. Dvali and A. Yu. Smirnov, Nucl.Phys. B563 (1999) 63.
- [9] K.R.S. Balaji, A. Perez-Lorenzana, A.Yu. Smirnov, Phys. Lett. B509:111, 2001.
- [10] S. M. Bilenky, C. Giunti, Phys. Lett. B320:323-328, 1994.
- [11] S. M. Bilenky, C. Giunti, Z.Phys. C68:495, 1995.
- [12] S. M. Bilenky, C. Giunti, Talk given at 4th International Workshop on Theoretical and Phenomenological Aspects of Underground Physics (TAUP 95), Toledo, Spain, 17-21 Sep 1995. Nucl.Phys.Proc.Suppl.48:381,1996, e-Print Archive: hep-ph/9512349.
- [13] Q. R. Ahmad *et al.*, SNO collaboration, Phys.Rev.Lett. 89: 011301 (2002).
- [14] Q. R. Ahmad *et al.*, SNO collaboration, Phys.Rev.Lett. 89: 011302 (2002).
- [15] V. Barger, D. Marfatia and K. Whisnant, Phys.Rev.Lett. 88 (2002) 011302
- [16] J. N. Bahcall, M. C. Gonzalez-Garcia, C. Peña-Garay, Phys.Rev. C66 (2002) 035802.

- [17] M. Maltoni, T. Schwetz, M.A. Tortola, J.W.F. Valle, hep-ph/0207227.
- [18] The idea to improve an upper bound on sterile fraction using KamLAND and solar neutrino results has been proposed by A. McDonald, July 2001, private communications.
- [19] CHOOZ Collaboration, M. Apollonio *et al.*, Phys.Lett. **B420**, 397 (1998).
- [20] BUGEY Collaboration, B. Achkar *et. al*, Nucl. Phys. **B434** (1995) 503.
- [21] P. C. de Holanda, A. Yu. Smirnov, hep-ph/0205241, to be published in Phys.Rev **D**.
- [22] B. T. Cleveland *et al* Astroph. J. **496** (1998) 505; K. Lande *et al*, in *Neutrino 2000* [23], p.50.
- [23] A. B. McDonald, Proc. of the 19th Int. Conf. on Neutrino Physics and Astrophysics, *Neutrino 2000* , Sudbury, Canada 2000, Nucl. Phys. B (Proc. Suppl.) **91** (2001) 21.
- [24] J.N. Abdurashitov et al. (SAGE collaboration), astro-ph/0204245.
- [25] C. M. Cattadori et al., in Proceedings of the TAUP 2001 Workshop, (September 2001), Gran-Sasso, Assesrgi, Italy.
- [26] S. Fukuda *et al.* (Super-Kamiokande collaboration) Phys. Rev. Lett. 86: 5651, 2001; Phys. Rev. Lett. 86: 5656, 2001.
- [27] Q. R. Ahmad *et al.*, SNO collaboration, Phys. Rev. Lett. 87:071301, 2001.
- [28] J. N. Bahcall, M.H. Pinsonneault and S. Basu, Astrophys. J. **555** (2001)990.
- [29] L. E. Marcucci *et al.*, Phys. Rev. **C63** (2001) 015801; T.-S. Park, *et al.*, hep-ph/0107012 and references therein.
- [30] KamLAND, P. Alivisatos, et. al., STANFORD-HEP-98-03, RCNS-98-15, 1998, S.A. Dazeley for the collaboration, hep-ex/0205041.
- [31] V. D. Barger, D. Marfatia, B. P. Wood, Phys. Lett. B498:53, (2001).
- [32] A. de Gouvea, C. Pena-Garay, Phys. Rev. D64:113011, (2001).
- [33] H. Murayama, A. Pierce, Phys.Rev.D65:013012,2002
- [34] M.C. Gonzalez-Garcia, C. Pena-Garay, Phys. Lett.B527:199, (2002).
- [35] P. Aliani, et. al., hep-ph/0211062.
- [36] P. C. de Holanda and A. Yu. Smirnov, in preparation.

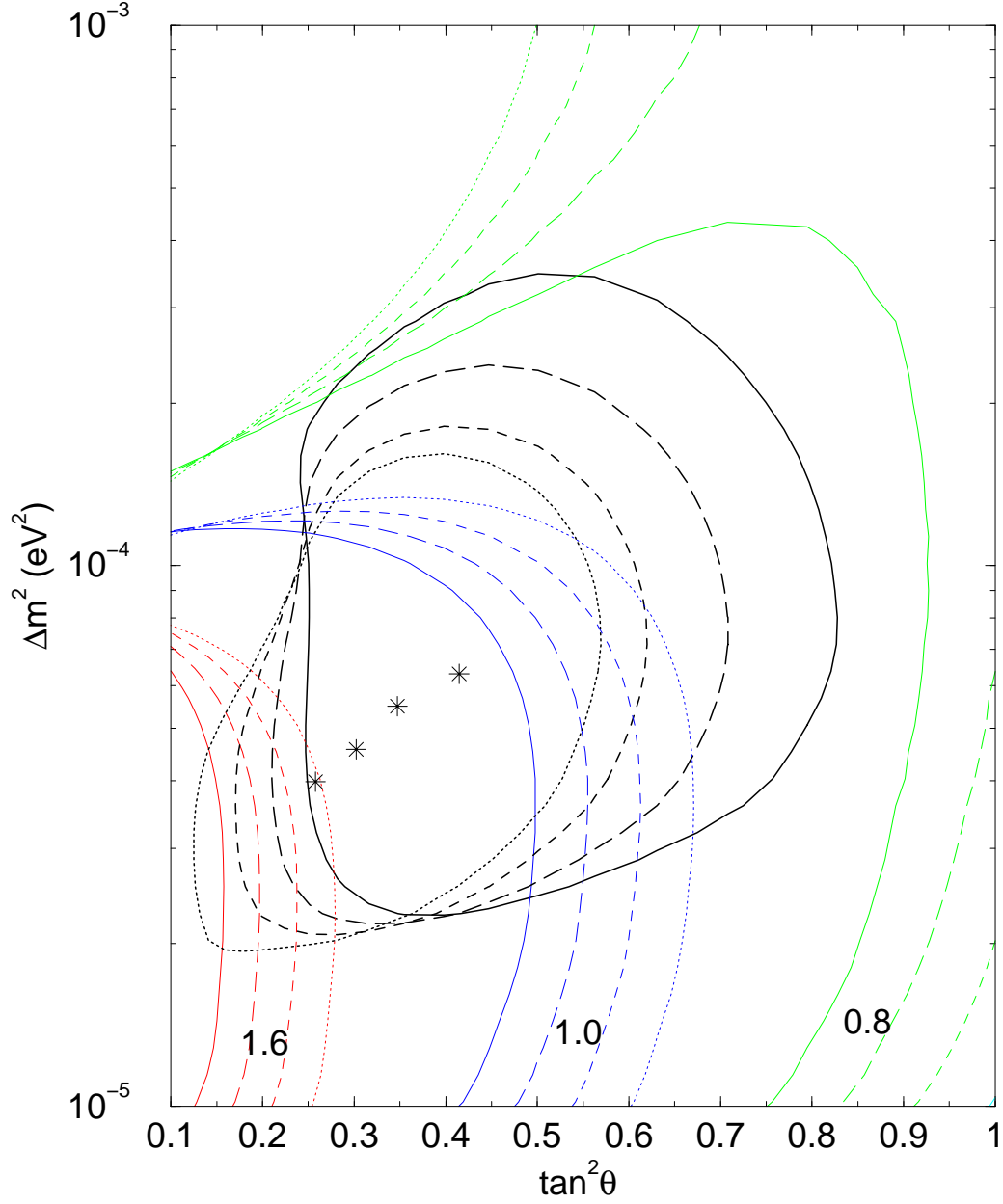


Figure 1: The best fit points and 3σ allowed regions of oscillation parameters for different values of η : $\eta = 0.0$ (solid line), 0.2 (long-dashed line), 0.4 (dashed line) and 0.6 (dotted line). Boron neutrino flux is taken as free parameters. Also shown lines of constant f_B which minimize χ^2 .

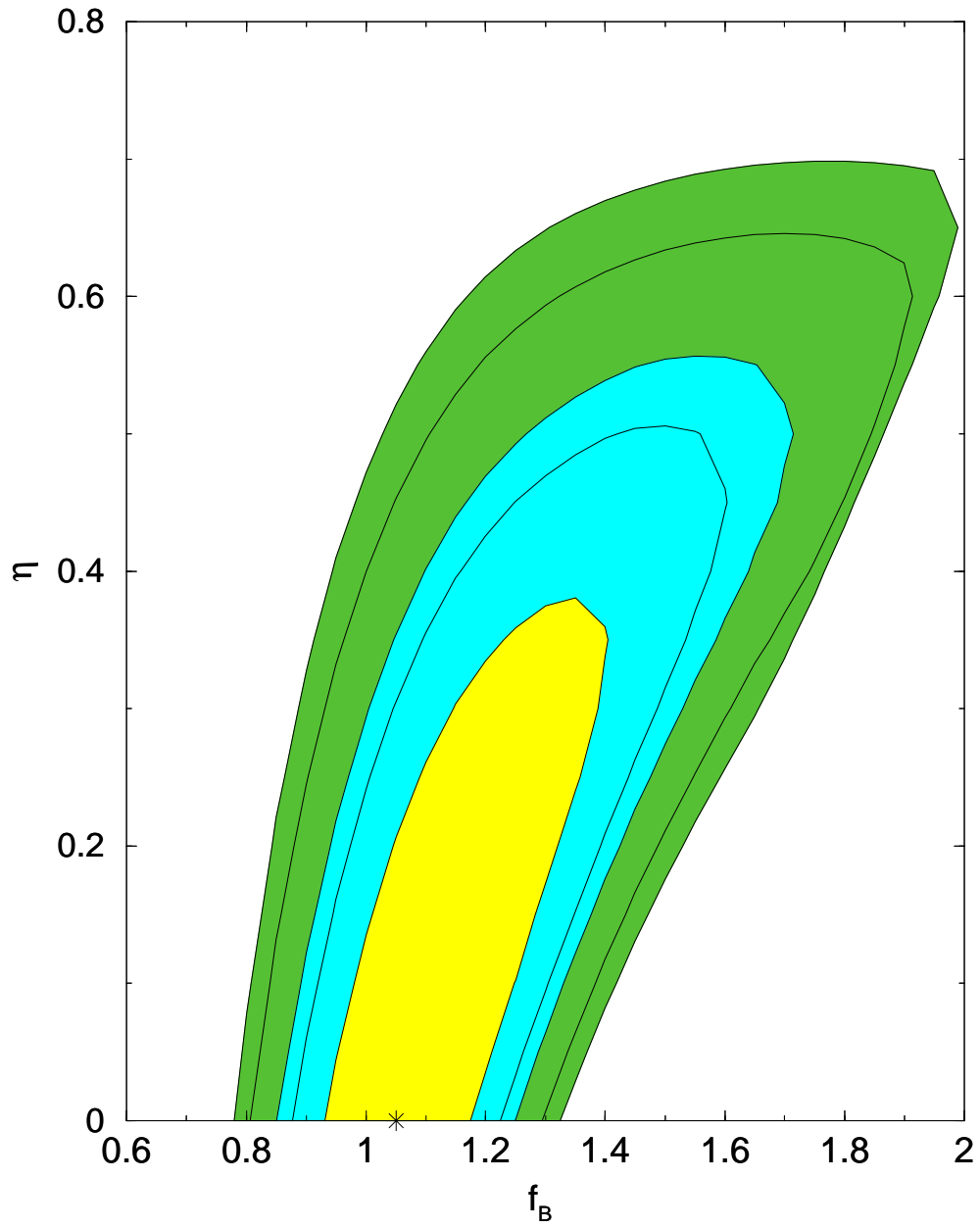


Figure 2: The allowed regions in $f_B - \eta$ plane, at 1σ , 90%, 95%, 99% and 3σ C.L.. The best fit point (marked by star) is at $\eta = 0$.

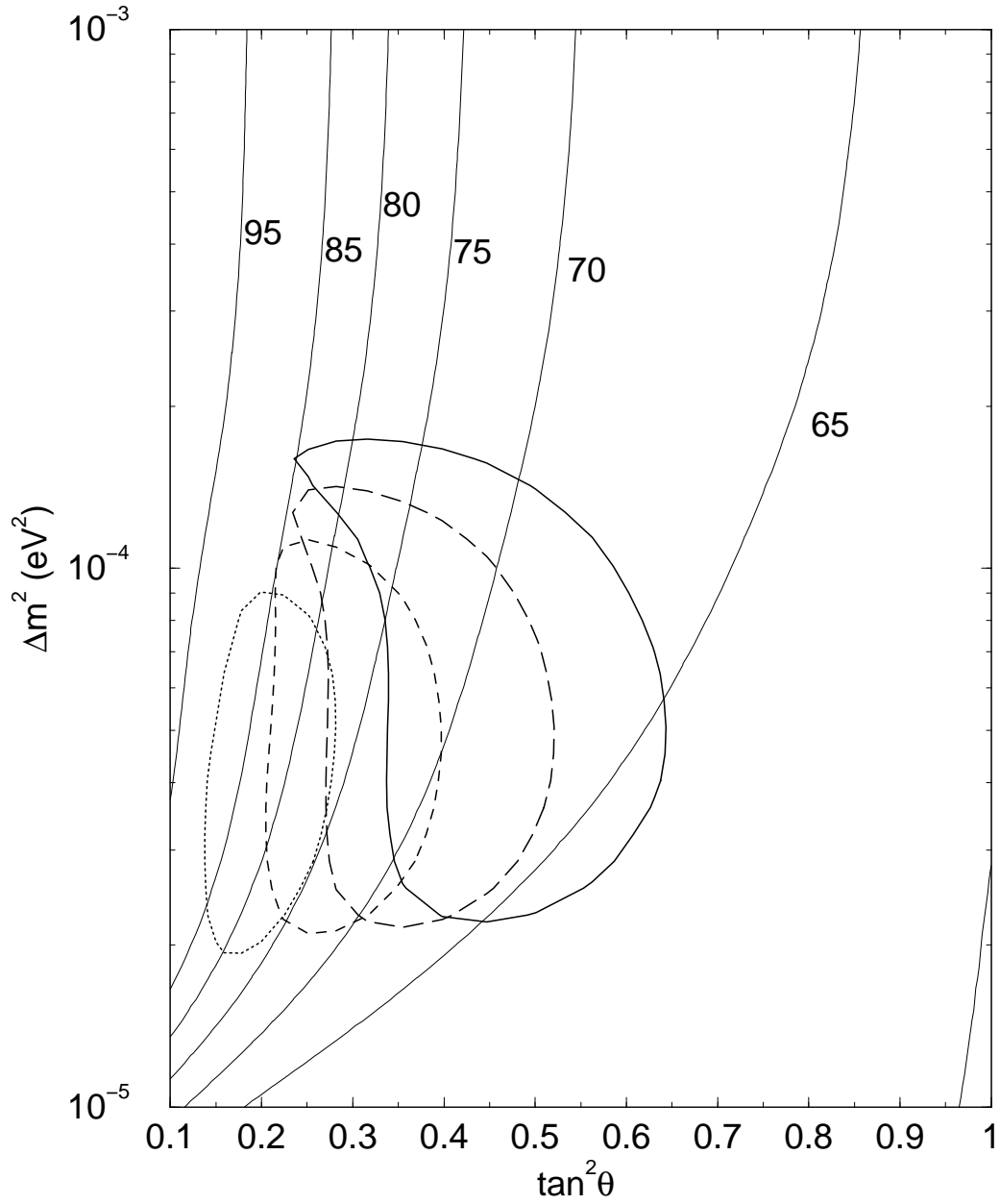


Figure 3: The 1σ allowed region from the analysis of the SNO data only for $\eta = 0$ (straight line), 0.2 (long dashed), 0.4 (dashed) and 0.6 (dotted). Also shown are lines of constant Q_{Ge} .

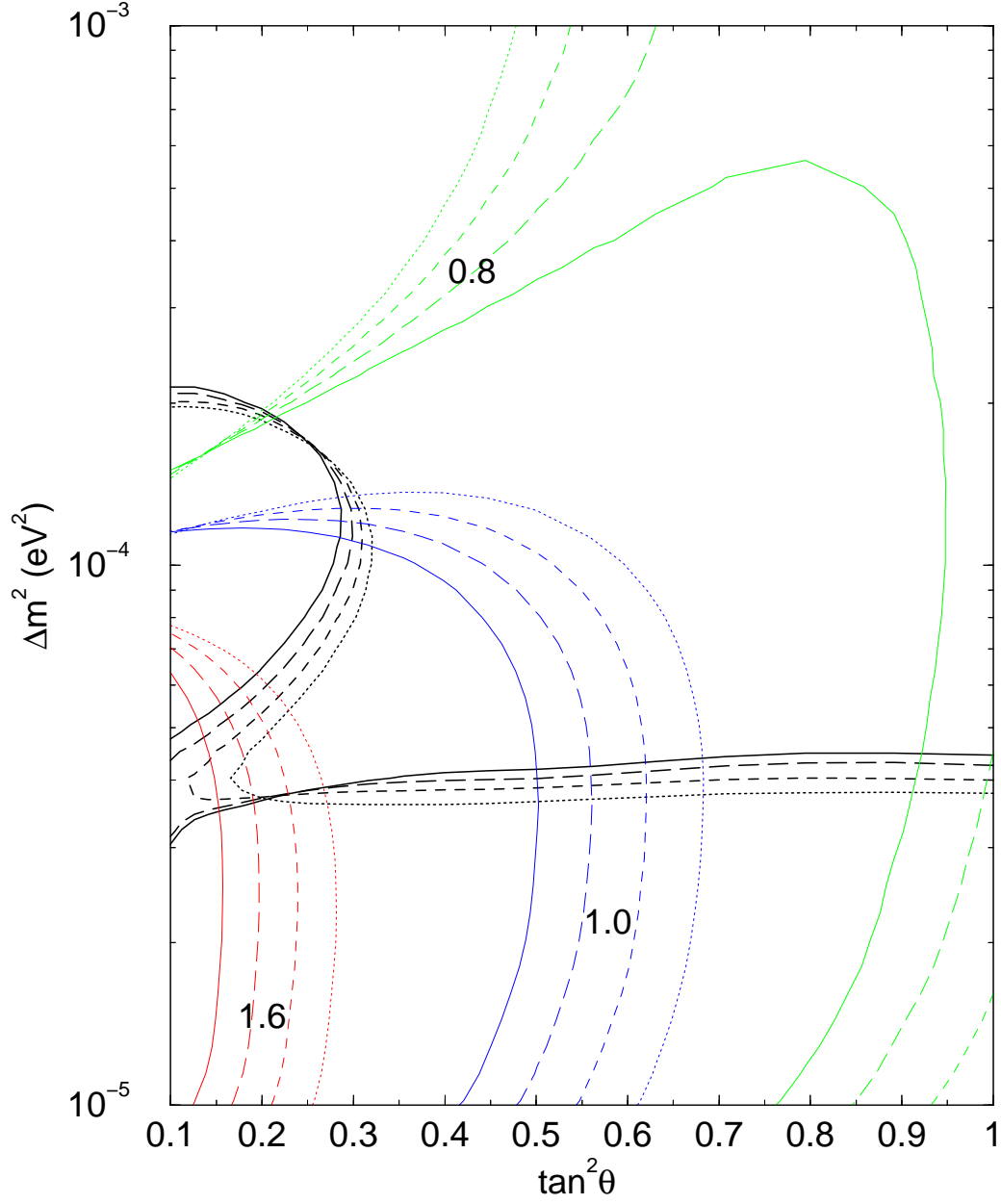


Figure 4: The 1σ allowed region (right upper parts) from the analysis of the SuperKamiokande data for different values of η . Also shown are lines of constant f_B which minimize χ^2 fit of the SK data for different η .

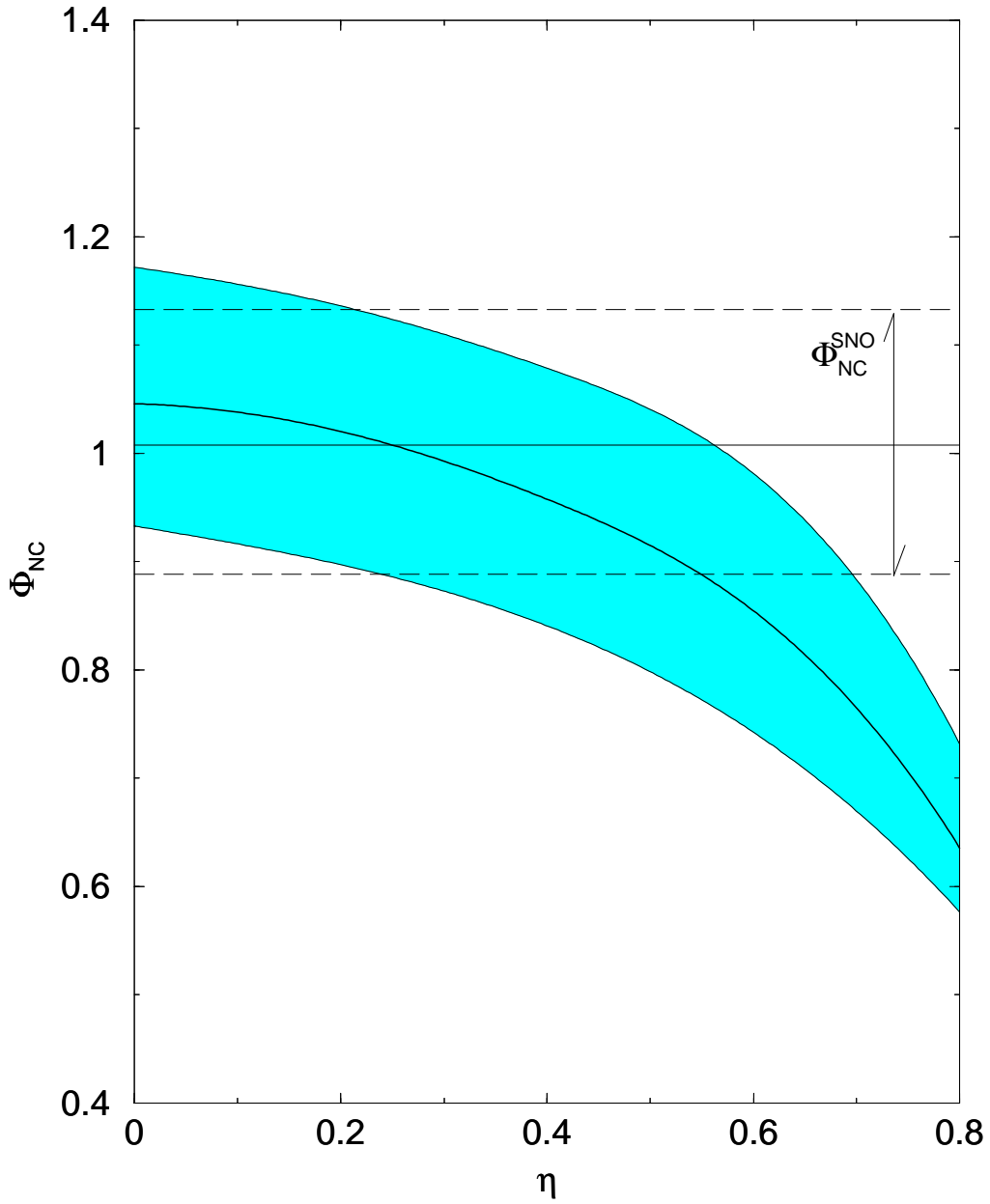


Figure 5: The predicted value of Φ_{NC} as a function of η . The band corresponds to the 1σ region. The horizontal lines show the present SNO result.

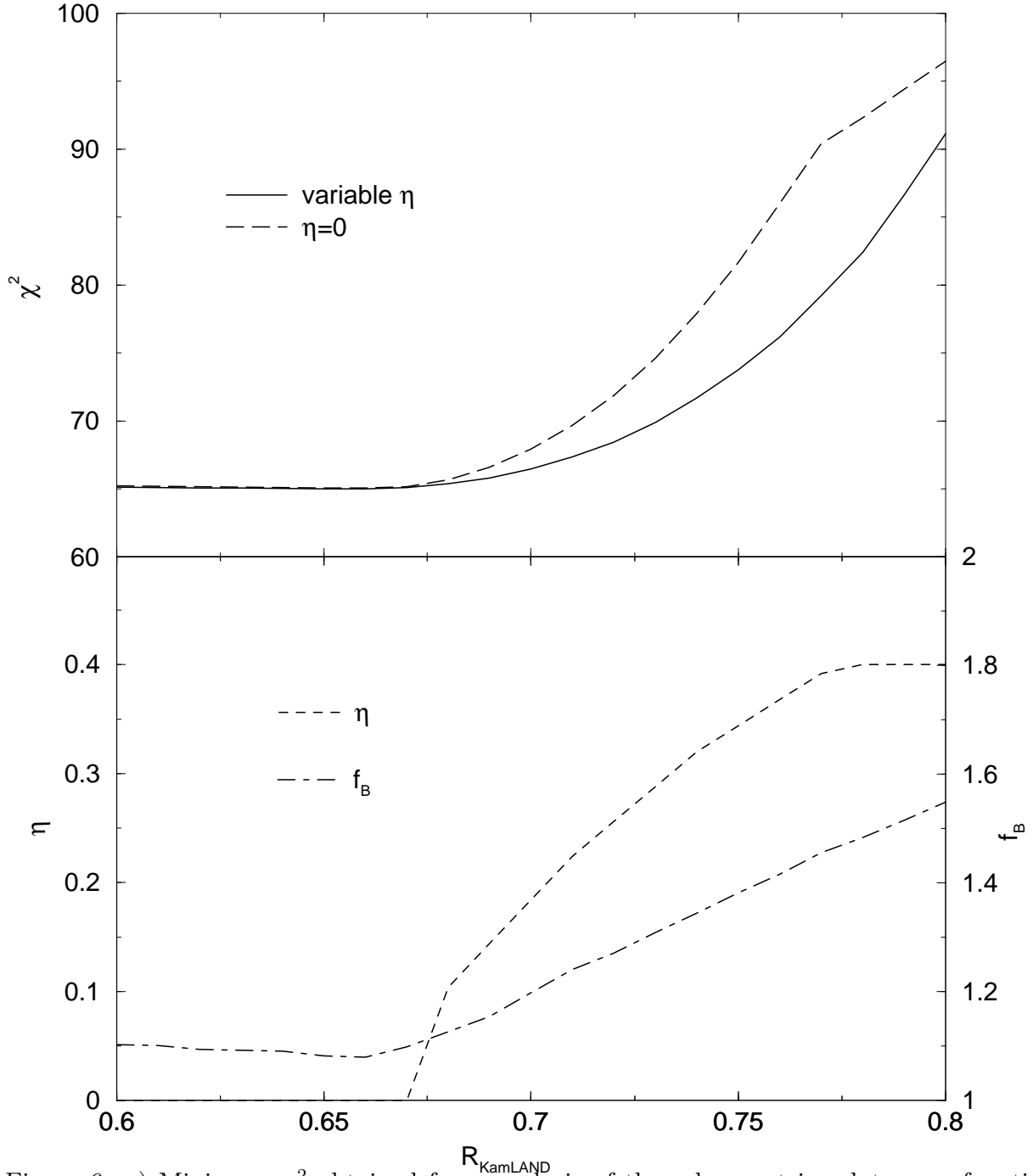


Figure 6: a) Minimum χ^2 obtained from analysis of the solar neutrino data as a function of the KamLAND rate, R_{KL} , $\eta = 0$ (dashed line) and for η taken as a free parameter (solid line). b) Value of η (solid line and left axis) and f_B (dashed line and right axis) that minimize the χ^2 presented in the panel a).

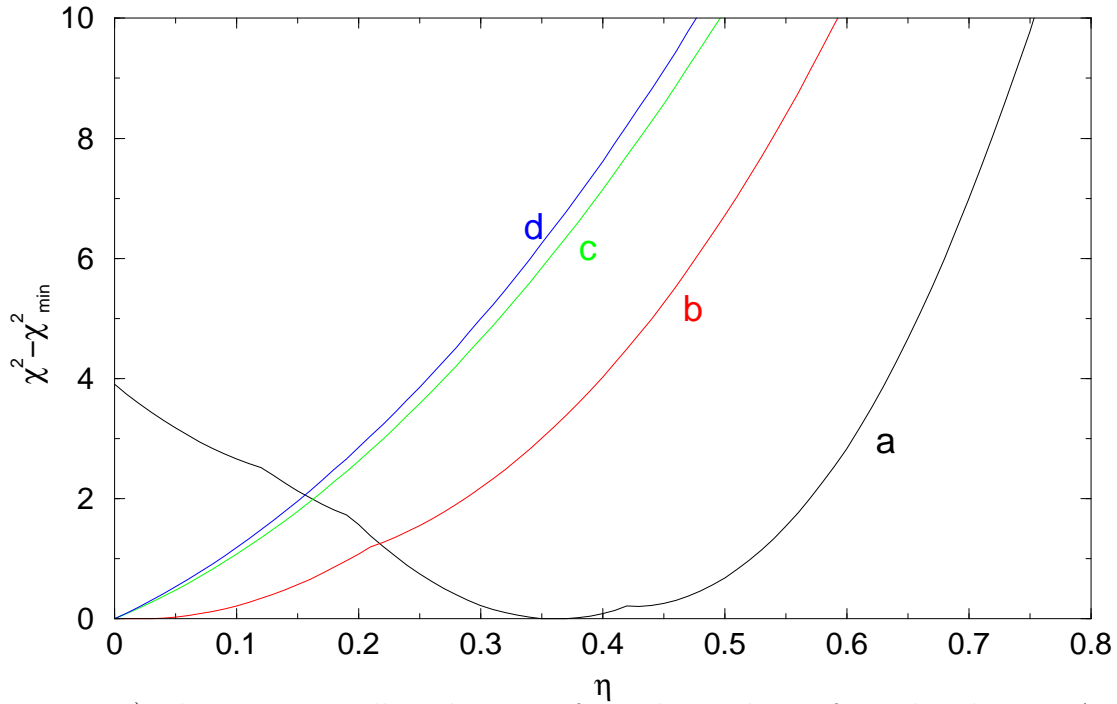
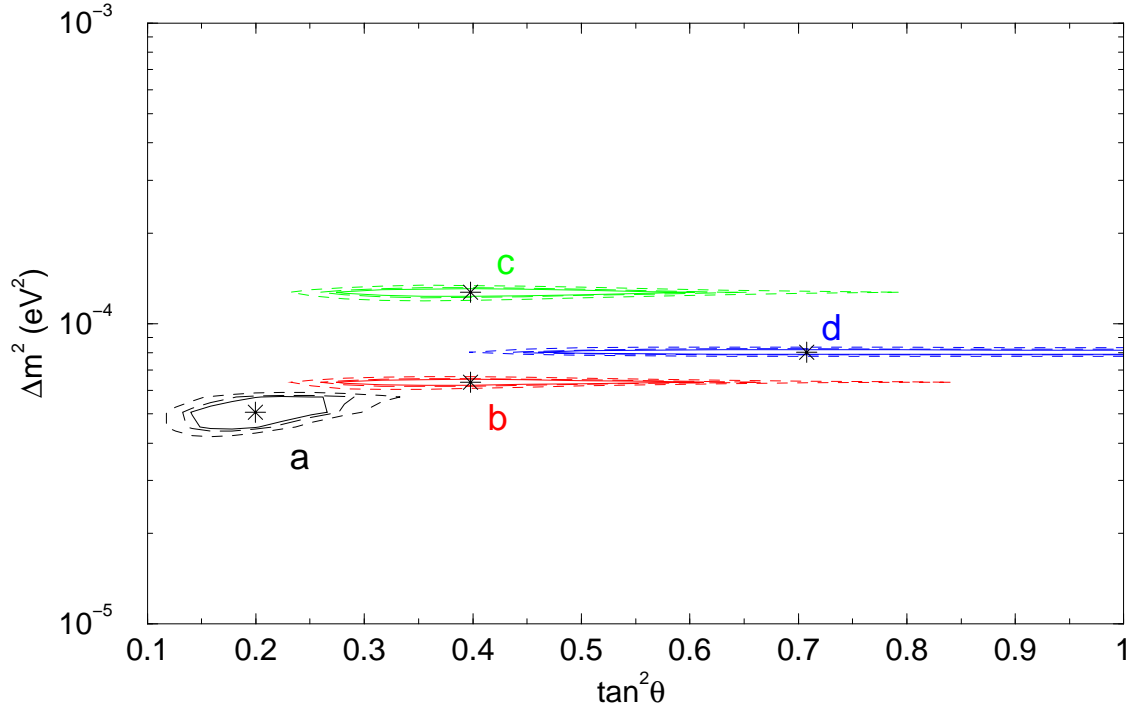


Figure 7: a) The 1σ , 2σ , 3σ allowed regions from the analysis of simulated KamLAND data. True values for the neutrino parameters that are indicated by a stars. b) The dependence of the χ^2 on η for these points from a combined analysis of the simulated KamLAND and the solar neutrino results.

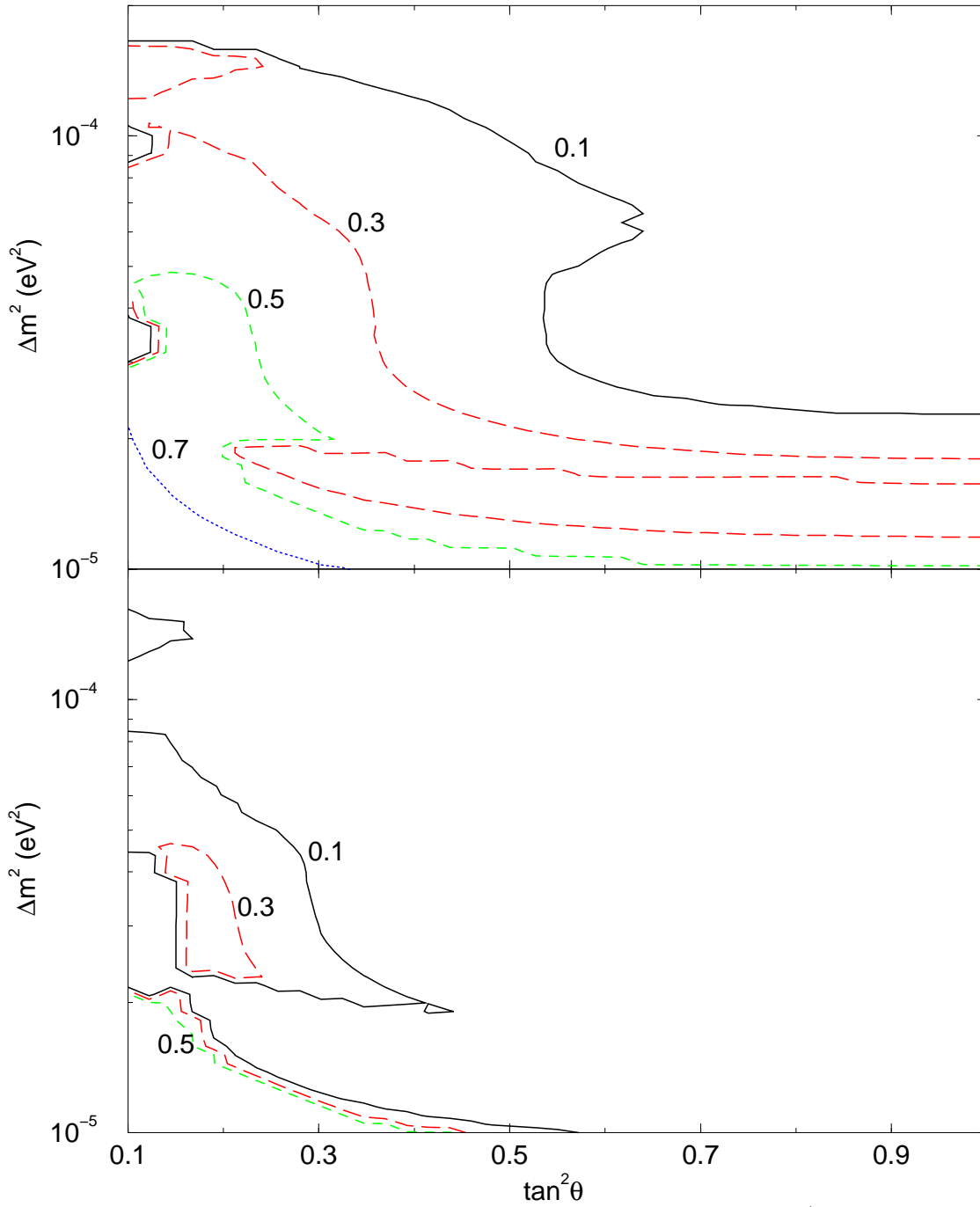


Figure 8: The upper panel: the lines of constant 1σ upper bound (figures at the curves) on η which can be obtained from from combined analysis of simulated KamLAND and solar neutrino results. The lower panel: the same as in the upper panel but for 1σ lower bound on η .